Available online at www.sciencedirect.com
SCIENCE DIRECT®
Journal of Catalysis 221 (2004) 365–377
JOURNAL OF CATALYSIS
www.elsevier.com/locate/jcat

Hydrodesulfurization of 4,6-dimethyldibenzothiophene over promoted (Ni,P) alumina-supported molybdenum carbide catalysts: activity and characterization of active sites

J.-M. Manoli,[a,*] P. Da Costa,[a] M. Brun,[b] M. Vrinat,[b] F. Maugé,[c] and C. Potvin [a]

[a] *Laboratoire Réactivité de Surface, CNRS UMR 7609, Case 178, Université P. et M. Curie, 4 place Jussieu, 75252 Paris cedex 05, France*
[b] *Institut de Recherches sur la Catalyse, CNRS UPR 5401, 2 av. A. Einstein, 69626 Villeurbanne cedex, France*
[c] *Laboratoire de Catalyse et Spectrochimie, CNRS UMR 6506, ENSICaen, Université de Caen, 6 boulevard du Maréchal Juin, 14050 Caen cedex, France*

Received 23 June 2003; revised 8 August 2003; accepted 8 August 2003

Abstract

The effect of phosphorus and nickel on alumina-supported molybdenum oxycarbides has been studied. Catalysts were characterized by elemental analysis, X-ray diffraction, CO chemisorption, transmission electron microscopy, energy-dispersive spectroscopy, X-ray photoelectron spectroscopy, and infrared spectroscopy. Propene and tetralin hydrogenation was used to probe the activity of the doped materials. Hydrodesulfurization of 4,6-dimethyldibenzothiophene (613 K and 4 MPa total pressure) was investigated as a probe for the deep HDS of diesel fuel. For contact times ranging from 0 to 0.4 s (conversion $< 45\%$), the HDS of 4,6-DMDBT is zero order with respect to the reactant and proceeds via two parallel routes, direct desulfurization and hydrogenation pathways, the former being preponderant. Phosphorus modifies catalytic behavior in several ways: increase in the Mo^{4+} abundance, increase in the number of Lewis acid sites, and consequent enhancement of the DDS rate. Nickel induces the highest HDS activity; a nickel–molybdenum interaction observed by FTIR spectroscopy of adsorbed CO could be responsible for this behavior.

Keywords: Molybdenum carbide; Hydrodesulfurization; 4,6-DMDBT; Phosphorus; Nickel; XPS; FTIR spectroscopy

1. Introduction

A future and more drastic specification for sulfur-containing diesel fuels (sulfur content as low as 50 wtppm by the year 2005 in Europe) is leading refiners to develop novel catalysts for deep desulfurization. To satisfy these demands for high-purity products, it is important to remove alkyl-substituted aromatic sulfur compounds. It is now well established that 4,6-dimethyldibenzothiophene (4,6-DMDBT) with alkyl groups near the sulfur atom is one of the most refractory [1–4].

Numerous studies recently reviewed [5,6] have been carried out in the last few years to better understand why such species are the most difficult to eliminate.

Hydrodesulfurization (HDS) of 4,6-DMDBT over commercial alumina-supported sulfided oxide catalysts (NiMoS/Al, CoMoS/Al) leads to two major compounds through two parallel reactions [7,8]: direct desulfurization (DDS), which yields dimethylbiphenyl (DMBP), and desulfurization with primary hydrogenation (HYD) of one ring of 4,6-DMDBT which gives methylcyclohexyltoluene (MCHT), a cyclohexylbenzene-type compound (Fig. 1). Moreover, it has been shown [5] that, over these types of catalysts, under deep HDS conditions DMBP does not hydrogenate to MCHT.

It is now agreed that after adsorption the dibenzothiophene molecule is first hydrogenated to dihydrodibenzothiophene [9–11]; a strong hydrogenating function is therefore necessary for this reaction. Around 80% of the HDS of 4,6-DMDBT goes by the hydrogenation route [10] with conventional alumina-supported sulfided oxide catalysts (NiMoS/Al, CoMoS/Al).

Hydrotreament catalysts often contain additives such as phosphates or fluorides [12,13]. It was claimed that phosphorus promotion [14] increases metal dispersion and modifies the distribution, the number, and the strength of acid

* Corresponding author.
E-mail address: jmm@ccr.jussieu.fr (J.-M. Manoli).

0021-9517/$ – see front matter
doi:10.1016/j.jcat.2003.08.011

sites, leading to good hydrogenation properties and therefore enhancing the HDS activity.

Most of these catalysts were used to transform nonrefractory compounds such as thiophene; few studies were performed with 4,6-DMDBT. Nevertheless, recently Kwak et al. [15] found that the effect of phosphorus (introduced as H_3PO_4 in the impregnating solution) on CoMoS/Al for the HDS of 4,6-DMDBT is to favor the DDS route. The authors attributed this trend to the enhancement of the Brønsted acidity.

Phosphorus can also be introduced onto the support directly by using heteropolyanions containing molybdenum, cobalt, and phosphorus with various Co/Mo ratios, followed by sulfidation [16,17]. These heteropolyanionic precursors improve thiophene HDS conversion. Conventional sulfided Co(Ni)Mo/Al catalysts have been much improved for HDS in the last decades but there is not yet a recognized alternative to these materials. Among studies on HDS over supported molybdenum carbide catalysts [18–23], we have examined 4,6-DMDBT [24]. Direct DDS is again favored, which contrasts with results for sulfided alumina-supported molybdenum oxides [25] under the same conditions. Recent research on phosphorus addition to bulk molybdenum carbides or nitrides [26] shows enhancement of the activity in the hydrogenation of unsaturated hydrocarbons. Insofar as a strong hydrogenating function is necessary in the HDS reaction, we have designed new alumina-supported carbides, containing phosphorus using heteropolyanions with defined P/Mo ratios. These new materials were characterized by FTIR spectroscopy and XPS measurements and tested for 4,6-DMDBT HDS. Finally, these materials were also compared with nickel-promoted carburized commercial catalysts.

2. Experimental

2.1. Materials

The support consisted of γ-alumina extrudates (Procatalyse, specific surface area $S_g = 180\ m^2\,g^{-1}$, total pore volume $V_p = 0.7\ cm^3\,g^{-1}$). For nonpromoted catalysts, commercial ammonium heptamolybdate $(NH_4)_6Mo_7O_{24} \cdot xH_2O$ (Acros) was used as precursor. For phosphorus-promoted catalysts, commercial $H_3PMo_{12}O_{40} \cdot xH_2O$ (Acros) and precursors such as $(NH_4)_6P_2Mo_{18}O_{62} \cdot xH_2O$ and $(NH_4)_6P_2Mo_5O_{23} \cdot xH_2O$, synthesized in the laboratory and described elsewhere [27,28], were used. Impregnated nickel-promoted catalysts (HR346C) were supplied by Procatalyse. Gases were CH_4, H_2, Ar, and O_2 (Air Liquide, 99.995%). Decalin (Aldrich, 99%) and 4,6-dimethyldibenzothiophene (Eburon Chemicals, 95%) were used as received.

2.2. Catalyst preparation

For nonpromoted catalysts, an incipient wetness impregnation was performed as described elsewhere [24,29] to obtain 10 wt% of Mo on the support.

For phosphorus-containing catalysts, phosphorus is introduced during the incipient wetness impregnation using heteropolyanions containing phosphorus and molybdenum. Two water-soluble heteropolyanions in the ammonium form, $(NH_4)_6P_2Mo_{18}O_{62} \cdot xH_2O$ (P/Mo = 0.11) and $(NH_4)_6P_2Mo_5O_{23} \cdot xH_2O$ (P/Mo = 0.40), were deposited on alumina to obtain 10 wt% of Mo on the support. A molybdenum carbide, with a P/Mo of 0.08 ratio was also synthesized, using an acidic precursor $H_3PMo_{12}O_{40} \cdot xH_2O$. Since this precursor is not very soluble, to achieve 10 wt% of Mo, four successive incipient wetness impregnations were necessary, depositing 2.5 wt% Mo in each step. After each step, the material was dried at 623 K overnight before a new impregnation. The alumina extrudates once impregnated were dried at 393 K for 12 h.

Molybdenum-based carbides (designated as Mo_2C/Al) were prepared by temperature-programmed carburization (TPC) according to previous publications [24,29]. Carbide synthesis was divided in two steps. First alumina-supported molybdenum extrudates were heated in argon for 8 h at 673 K with a flow rate of 60 $cm^3\,min^{-1}$. The material was then carburized by TPC in flowing CH_4/H_2 (20% v/v mixture, total flow rate: 60 $cm^3\,min^{-1}$), the temperature being raised linearly from 673 to 950 K. At this final temperature the CH_4/H_2 flow was switched to hydrogen and the materials were cooled to room temperature for 1 h. After cooling, the supported carbides were passivated with 1% O_2/Ar (v/v) at room temperature for about 1 h before characterization and catalytic runs.

An alumina-supported nickel carbide, noted NiC/Al, was synthesized using the same procedure as for supported molybdenum-based carbides. Ni oxide/Al was reduced in hydrogen flow to obtain a similar material with identical nickel content.

For nickel-promoted catalysts, alumina-supported commercial oxide, NiMo oxide/Al, was used. The drying step is not performed on this material before carburization, and the material is designated as $NiMo_2C$/Al. For the sake of comparison, a nickel-based catalyst was synthesized with a Ni content similar to $NiMo_2C$/Al and noted Ni/Al.

Extrudates of supported carbides were ground and sieved to obtain particle sizes between 0.25 and 0.4 mm. Samples are denoted $Mo_2CP(X)$/Al, X being the theoretical P/Mo atom ratio. Table 1 summarizes the catalysts used in this study.

In addition, two Mo carbides supported on silica (provided by Grace) were prepared; these are denoted Mo_2C/Si and $Mo_2CP(0.4)$/Si and are used only for the IR study in order to avoid any contribution of the support to the acidity of the system. They were carburized by the standard procedure.

2.3. Hydrodesulfurization of 4,6-DMDBT

The reaction was carried out at 613 K and a total pressure of 4 MPa; 4,6-DMDBT was diluted in decalin, the mixture being injected by a high-pressure pump (Gilson,

Table 1
Catalysts, precursors, and pH of impregnation solutions

Catalyst	Precursor	pH	Source	Treatment
Mo_2C/Al	$(NH_4)_6H_2Mo_7O_{24} \cdot xH_2O$	3.9	Acros	I/C[b]
Mo_2CP(0.08)/Al	$H_3PMo_{12}O_{40} \cdot xH_2O$	1.2	Acros	I/C
Mo_2CP(0.11)/Al	$(NH_4)_6P_2Mo_{18}O_{62} \cdot xH_2O$	3.9	Home-made[a]	I/C
Mo_2CP(0.40)/Al	$(NH_4)_6P_2Mo_5O_{23} \cdot xH_2O$	4.2	Home-made[a]	I/C
NiMo_2C/Al	–	–	Procatalyse	C
NiC/Al	$Ni(NO_3)_2 \cdot 6H_2O$	3.8	Fluka	I/C
Ni/Al	$Ni(NO_3)_2 \cdot 6H_2O$	3.8	Fluka	I/R

[a] Synthesis from Refs. [27,28].
[b] I, impregnated; C, carburized; R, reduced.

Model 307). Under standard reactions the various partial pressures were 4,6-DMDBT, 0.001 MPa; decalin, 0.888 MPa; and hydrogen, 3.111 MPa. The ratio of H_2 flow/liquid feed flow was set to 500. Before reaction, 0.4 g of supported carbides was pretreated in situ, at 423 K and 4 MPa in flowing hydrogen (100 $cm^3\,min^{-1}$) for 1 h. Then feedstock was introduced and the temperature raised to 613 K. The liquid products of the reaction were periodically collected (every hour) and analyzed by gas chromatography (Varian 3400) using a flame ionization detector and a capillary column (DB1). All the quantitative chromatographic analyses were performed by using an external standard, namely 1-methylnaphthalene.

The partial pressure of H_2S depends on the hydrodesulfurization conversion and ranged from 0 to 0.0009 MPa, corresponding to 90% conversion of 4,6-DMDBT. For each run, so for each contact time, a new sample of catalyst was used, to avoid any influence of the feedstock on the carbide.

The kinetics were studied with contact times up to 2 s. The contact time is defined as the catalyst volume (cm^3) divided by the total feed flow rate ($cm^3\,s^{-1}$).

2.4. Hydrogenation catalyst characterization

2.4.1. High-pressure hydrogenation

Tetralin was chosen as a probe for the hydrogenation of aromatics in diesel fuels [24,29,30]. The reaction was carried out at 573 K and a total pressure of 4 MPa. Tetralin was diluted in *n*-heptane, the mixture being injected by a high-pressure pump. Partial pressures of tetralin, *n*-heptane, and hydrogen were 0.01, 0.93, and 3.06 MPa, respectively. The products of the reaction were collected periodically (every hour) and analyzed on a 50-m capillary column (HP Pona). Before reaction, 0.2 g of supported carbides were pretreated in situ, at 423 K and 4 MPa in flowing hydrogen (17 $cm^3\,min^{-1}$) to remove the passivation layer. Under our experimental conditions, the only products of transformation were *cis*- and *trans*-decalin (hydrogenation products) and a small amount of naphthalene (dehydrogenation product), as already reported for alumina-supported catalysts [24].

2.4.2. Atmospheric pressure hydrogenation

Following Burwell [31] propene hydrogenation (a structure-insensitive reaction) was used to determine the properties of materials at atmospheric pressure. The reaction was carried out in a flow reactor at 250 K. The gas mixture (the H_2/C_3H_6 molar ratio was fixed at 6.7 and the total flow rate at 117 $cm^3\,min^{-1}$) was fed into a Pyrex reactor loaded with 0.1 g of catalyst on a sintered glass disk (diameter 1 cm). The effluent was analyzed with a HP 5890 Series II gas chromatograph equipped with a KCl-modified Al_2O_3 capillary column and a flame ionization detector. The only product observed was propane. Prior to each run, passivated catalysts were pretreated in situ at 773 K in flowing H_2 (12 $cm^3\,min^{-1}$) for 4 h. As the catalysts suffered deactivation during reaction, the reciprocal value of the conversion τ versus time of run t was used to determine the initial conversion τ_0 by extrapolation to zero time: $1/\tau = 1/\tau_0 + \kappa$ where κ is an empirical deactivation constant [32].

2.5. X-ray photoelectron spectroscopy

X-ray photoelectron spectra were recorded with a VG Scientific, Escalab 200R spectrometer equipped with a Mg-K_α X-ray source and a hemispherical analyzer. In the case of Ni-containing compounds an Al-K_α source was used. Sealed glass tubes containing the materials were opened in a glove box (dry argon) and introduced into the spectrometer chamber without exposure to air. The vacuum during the measurements was typically less than 5×10^{-6} Pa and the scan speed 0.02 eV/s with 0.1 eV $step^{-1}$. The Al 2p line of Al_2O_3 at 74.0 eV was taken as reference in calculating binding energies and accounting for the charging effect. Experimental peaks were decomposed into components using mixed Gaussian–Lorentzian functions and a nonlinear least-squares fitting algorithm; Shirley background subtraction was applied. An intensity ratio of 2/3 and a splitting of 3.2 eV was used to fit the Mo 3d peaks. The surface composition (in atom percent) of the various samples was determined from the integrated peaks of C 1s, O 1s, Mo 3d, P 2p, and Ni 2p using their respective experimental sensitivity factors [33]. Binding energies (BE) were reproducible to within ± 0.2 eV.

2.6. FTIR measurements

The passivated catalyst powders were pressed into self-supported wafers (ca. 5 $mg\,cm^{-2}$, diameter = 1.6 cm) and

retreated in situ in the IR cell. The wafer was pumped down to 10^{-2} Pa, the temperature being raised from RT to 773 K at 4 K min^{-1} and then held at 773 K for 30 min. Then three cycles of hydrogen contact ($P_{H_2} = 2.7 \times 10^4$ Pa; contact time = 1, 2, and 1 h) at 773 K followed by evacuation at the same temperature were performed, the last evacuation being prolonged until the residual pressure in the cell reached 3×10^{-3} Pa. The activated catalysts were either (1) equilibrated with 267 Pa of pyridine at RT and evacuated at 473 K or at RT or (2) equilibrated with 1.333×10^3 Pa of CO and evacuated all at RT. In an additional experiment, the activated catalyst was treated with 133 Pa H_2O at RT. The IR spectra were recorded at RT using a Nicolet 60SX FTIR spectrometer. For comparison, spectra and band area values presented in this work were normalized to a disk of 5 mg cm^{-2}.

2.7. Dispersion measurements

The passivated catalysts, before and after reaction, were characterized by XRD, CO chemisorption, transmission electron microscopy (TEM), and EDS analysis. Powder X-ray diffraction (XRD) was carried out on a Siemens Model D-500 diffractometer with Cu-K_α radiation. The selective chemisorption of CO was used to titrate the number of active metal sites before runs and was performed by a pulse technique at 293 K. Titration was carried out by passing a known volume of CO controlled by an automatic valve through a quartz reactor containing the material (0.3 g), He being used as carrier gas. A catharometer cell detected the remaining nonadsorbed CO at the outlet of the reactor. Prior to chemisorption, the passivated promoted or nonpromoted catalyst was reduced in flowing H_2 (12 cm^3 min^{-1}) at 773 K for 4 h, purged in flowing He for 0.5 h, and then quenched at 293 K. High-resolution transmission electron microscopy (HRTEM) was used to determine the particle size of molybdenum carbides supported on alumina and to check their dispersion. HRTEM studies were performed on a Jeol-JEM 100 CXII apparatus associated with a top-entry device and operating at 100 kV. Energy dispersive spectroscopy (EDS) analysis (STEM mode) was performed with the same apparatus using a Link AN 10000 system, connected to a silicon–lithium diode detector and multichannel analyzer. The EDS analyses were obtained from large domains of samples (from 150×200 to 400×533 nm^2). Elemental analysis (Mo, P, Ni, C) was performed by the Service Central d'Analyses du CNRS on fresh and spent catalysts.

3. Results and discussion

3.1. Effect of promoter on the dispersion of supported molybdenum carbide catalysts

TEM and EDS measurements were performed to estimate the particle size of molybdenum carbides. TEM showed no particles on alumina-supported molybdenum carbide, in contrast to alumina-supported tungsten carbides described elsewhere [29]. On alumina-supported carbides promoted by nickel, no particles were observed either.

Table 2
EDS measurements and elemental analysis of alumina-supported molybdenum carbides

Catalyst	Mo/Al	P/Mo			Ni/Mo	C/Mo
		Theoretical	E.A.[a]	EDS[b]		
Mo_2C/Al	0.070				–	0.35
Mo_2CP(0.08)/Al	0.068	0.08	0.08	n.m.[c]	–	0.31
Mo_2CP(0.11)/Al	0.069	0.11	0.11	0.12	–	0.30
Mo_2CP(0.40)/Al	0.067	0.40	0.39	0.41	–	0.31
$NiMo_2C$/Al	0.063	–		–	0.23	0.30

[a] Elemental analysis (CNRS).
[b] Energy-dispersive spectroscopy.
[c] n.m., not measured.

The specific content of molybdenum, nickel, and phosphorus was evaluated by EDS (Table 2). For all the catalysts, the molybdenum content does not change whatever the area analyzed, which indicates that the molybdenum is very well dispersed on the support. The phosphorus is also well dispersed and, on the scale of the domains examined, the P/Mo ratios are close to those in the heteropolyanion structure. Moreover, EDS analysis shows that after carburization, the situation is the same; hence the use of the heteropolyanion complexes leads to a proximity of the P and Mo atoms.

EDS measurements showed also there is no nickel migration in the support, the Ni/Mo ratios remaining constant and close to the value found for commercial HR346C. These results indicate that there is a homogeneous distribution of the molybdenum carbides on the alumina support.

X-ray diffraction leads to the same conclusions. For 10 wt% Mo, alumina-supported molybdenum carbide particles are not detected by XRD, which means that the particles of Mo_2C are well dispersed on the support. The presence of phosphorus does not affect these conclusions. For alumina-supported $NiMo_2C$/Al catalysts, no characteristic peaks of mixed NiMo carbide phases, Ni_3C, or a metallic nickel phase were detected by XRD, contrary to the results of Xiao et al. [34] on the corresponding bulk bimetallic molybdenum–cobalt carbides. These observations are consistent with the work of Bussell et al. [35] and allow us to conclude that the carbide domains are very small and highly dispersed on the alumina support.

3.2. Titration of surface metal atoms

The chemisorption of CO has been used to characterize alumina-supported molybdenum carbides [18,35,36]. As shown in Table 3, the CO uptakes of the samples examined range from 26 to 45 μmol g^{-1}. For the supported molybdenum carbides the values are smaller than those reported [18,35–37], the material synthesized from the P/Mo = 0.4 precursor having a lower CO uptake (26 μmol g^{-1}) than the catalyst without any additive. No correlation can be observed

Table 3
CO chemisorption, surface area measurements, and activity in propene hydrogenation at 250 K

Catalyst	S_g ($m^2\,g^{-1}$)	Chemisorbed CO ($\mu mol\,g^{-1}$)	Initial conversion (%)
Alumina	191	0	0
Mo_2C/Al	171	40	3.0
Mo_2CP(0.08)/Al	168	45	6.1
Mo_2CP(0.11)/Al	167	41	16.1
Mo_2CP(0.40)/Al	168	26	19.8
$NiMo_2C$/Al	165	44	77.9
NiC/Al	178	–	82.7
Ni/Al	180	–	94.1

between P content and CO uptake, nor between the different promoters and CO uptake.

For the Ni-promoted catalyst $NiMo_2C$/Al, the chemisorption capacity is slightly higher than that measured on Mo_2C/Al. For a similar molybdenum loading Bussell et al. [35] observed greater CO uptake for Co-promoted alumina-supported molybdenum carbides (86 $\mu mol\,g^{-1}$) as against 69 $\mu mol\,g^{-1}$ for Mo_2C/Al. These discrepancies are certainly due to the alumina support and to the different impregnation and carburization procedures used by Bussell et al. Furthermore, the CO chemisorption behavior of nickel in $NiMo_2C$/Al is not known. Measurements (Table 3) indicate that for no catalyst carburization affects the surface area; the decrease in S_g during synthesis is not significant.

3.3. Hydrogenation properties

Propene hydrogenation was selected as a test reaction to evaluate the role of phosphorus on the activity of our materials at atmospheric pressure. As reported in Table 3, the P-containing catalysts had higher hydrogenation activity, as indicated by the values of the initial conversion at 250 K. As already noted for bulk catalysts [26], the presence of phosphorus is closely related to the hydrogenation character of the molybdenum carbides. All the Ni-based or Ni-promoted alumina-supported catalysts have better hydrogenation properties than P-promoted catalysts, with initial conversions of 78–94 and 6–20%, respectively. The initial conversions of NiC/Al and $NiMo_2C$/Al are comparable but these carburized catalysts are rapidly deactivated, contrary to Ni/Al.

The catalysts were also tested in tetralin hydrogenation at 573 K and high pressure (4 MPa) under conditions similar to those of the HDS reaction. Activities were enhanced by phosphorus addition (Fig. 1) at high pressure.

3.4. Reactivity of promoted alumina-supported molybdenum carbides in 4,6-DMDBT HDS

3.4.1. Kinetic results

It is well known that the HDS of 4,6-DMDBT on sulfided alumina-supported molybdenum oxides leads to methylcyclohexyltoluene and dimethylbiphenyl, via two parallel pathways, HYD and DDS (Fig. 2) [7,10,38–40]. With

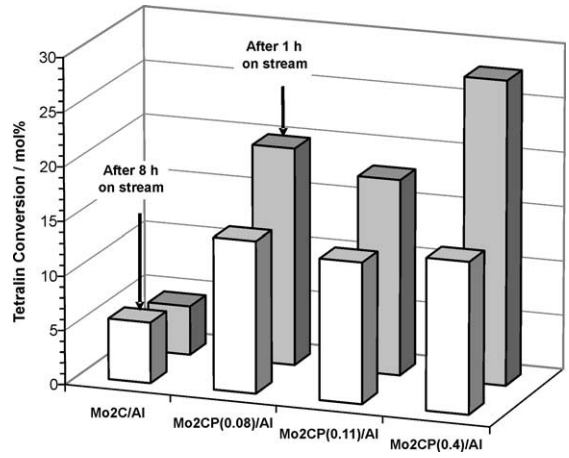

Fig. 1. Tetralin conversion (573 K, 4 MPa total pressure) on P-doped alumina-supported molybdenum carbides: evolution with time on stream (1 h first analysis, 8 h steady state).

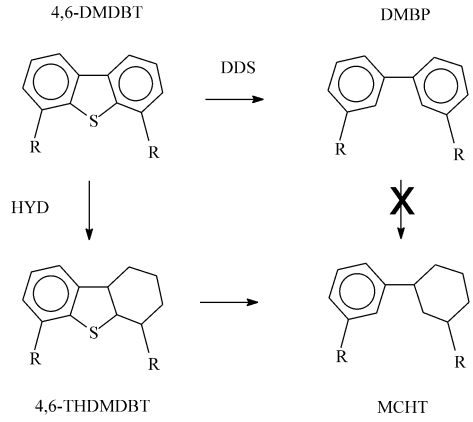

Fig. 2. Hydrodesulfurization of 4,6-DMDBT (R = CH_3), DDS, direct desulfurization; HYD, hydrogenation.

Mo_2C/Al, we showed [24] that the HDS products, DMBP and MCHT, are independent for conversions lower than 45%. In fact, DMBP is never hydrogenated to MCHT in the HDS reaction [41]. We proposed a mechanism for carbide catalysts in agreement with that for sulfided catalysts [10].

Kinetic study of 4,6-DMDBT hydrodesulfurization [24] showed that for an alumina-supported molybdenum carbide, Mo_2C/Al, two kinetic domains exist depending on the contact time or on the 4,6-DMDBT conversion. At low contact time (i.e., conversion lower than 45%), an overall zero order was found for the reaction. The adsorbed 4,6-DMDBT, [DMDBT*], saturates the surface. It is assumed to be the most abundant surface intermediate (MASI) [42]; the other species can be neglected and therefore [DMDBT*] is equal to the total number of sites, $[L]$. In this case, the expression of the overall reaction rate r_{HDS} is the sum [Eq. (1)] of the DDS (r_{DDS}) and HYD (r_{HYD}) rates

$$r_{HDS} = (k_{1H,H_2} + k_{1D})[\text{DMDBT}^*] = k_1[L], \quad (1)$$

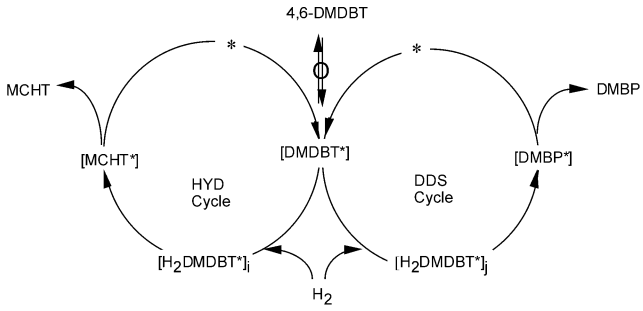

Fig. 3. Coupled catalytic cycles for hydrodesulfurization of 4,6-DMDBT over alumina-supported molybdenum carbides: [DMDBT*], adsorbed 4,6-DMDBT; [MCHT*], adsorbed MCHT (HYD product); [DMBP*], adsorbed DMBP (DDS product); *, free active site.

where k_{1H,H_2} is the first rate constant of the HYD route and k_{1D} the rate constant of the first elementary step in the direct DDS route, in which r_{DDS} and r_{HYD} appear, according to

$$r_{HDS} = r_{HYD} + r_{DDS} = k_1[L]. \quad (2)$$

The rates of MCHT (r_{HYD}) and DMBP (r_{DDS}) formation, expressed in moles of products per gram of catalyst, are calculated at low contact times (< 0.4 s). The kinetic study leads us to propose two coupled catalytic cycles (Fig. 3) with one common adsorbed species, [DMDBT*]. In each cycle the first elementary step is a dihydrogenation of the reactant leading to a dihydrogenated derivative of 4,6-DMDBT, adsorbed H_2DMDBT. According to Bataille et al. [10] nine dihydroisomers can be formed through partial hydrogenation of 4,6-DMDBT. Of these species only two (noted $[H_2DMDBT^*]_j$ in the adsorbed state) can lead to the DDS pathway, all the others, abbreviated as $[H_2DMDBT^*]_i$, leading to the HYD pathway.

Fig. 4 displays moles of reactant and products versus contact time, expressed for two catalysts taken as examples, a P-promoted alumina-supported catalyst ($Mo_2CP(0.4)/Al$) and a Ni-promoted alumina-supported catalyst ($NiMo_2C/Al$). Two zones can be observed for all catalysts, which can be compared for experiments at low contact time. We consider MCHT and DMBP as primary products, for the DDS and HYD reactions, respectively, and 4,6-DMDBT as the reactant for the overall HDS reaction. The zero-order domain depends on the catalyst, but changes in the kinetic order of the reaction never appear before an HDS conversion of about 50%.

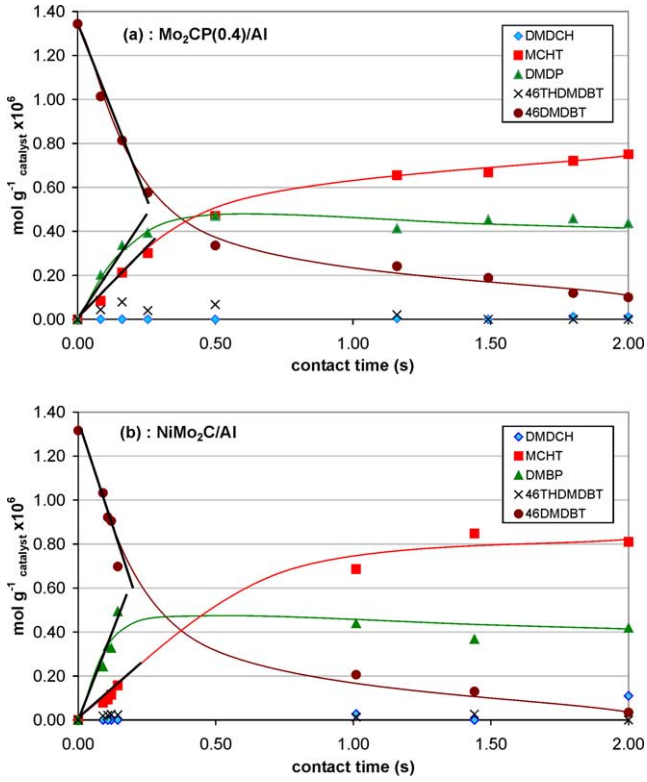

Fig. 4. Hydrodesulfurization of 4,6-DMDBT over Mo_2C/Al: moles of reactant and products per gram of catalyst versus contact time (a) on $Mo_2CP(0.4)/Al$, and (b) on $NiMo_2C/Al$.

3.4.2. Promotion effect on the HDS rates

In Fig. 4 the straight lines are plotted at low contact times, and these linear plots for 4,6-DMDBT transformation and for DMBP and MCHT formation are characteristic of zero-order reactions; the kinetic results are presented in Table 4. The overall HDS rate, measured at low contact times, is enhanced with P-doped alumina-supported molybdenum carbides [37]. The HDS rate increases with the phosphorus content, if we consider the same type of nonacidic precursors as presented in Table 1. Rates range from 1.87×10^{-6} mol g^{-1} s^{-1} for Mo_2C/Al to 3.31×10^{-6} mol g^{-1} s^{-1} for $Mo_2CP(0.40)/Al$. The selectivity ratio of the reaction defined as the rate ratio, r_{HYD}/r_{DDS}, ranges from 0.4 to 0.7. Phosphorus leads to an enhancement of the overall HDS.

A similar positive effect was observed for HDS of dibenzothiophene by Dhandapani et al. [37] with Mo_2C/Al-P (the support had been treated with $(NH_4)_2HPO_4$ before im-

Table 4
Rate and selectivity ratio in HDS of 4,6-DMDBT on alumina-supported molybdenum carbides: effect of P, Ni

Catalyst	r_{HDS} (mol g^{-1} s^{-1}) $\times 10^6$	r_{HYD} (mol g^{-1} s^{-1}) $\times 10^6$	r_{DDS} (mol g^{-1} s^{-1}) $\times 10^6$	r_{HYD}/r_{DDS}
Mo_2C/Al	1.87	0.76	1.10	0.7
$Mo_2CP(0.08)/Al$	3.81	1.14	2.74	0.4
$Mo_2CP(0.11)/Al$	2.50	0.86	1.58	0.5
$Mo_2CP(0.40)/Al$	3.31	1.25	1.83	0.7
$NiMo_2C/Al$	4.10	1.03	3.11	0.3

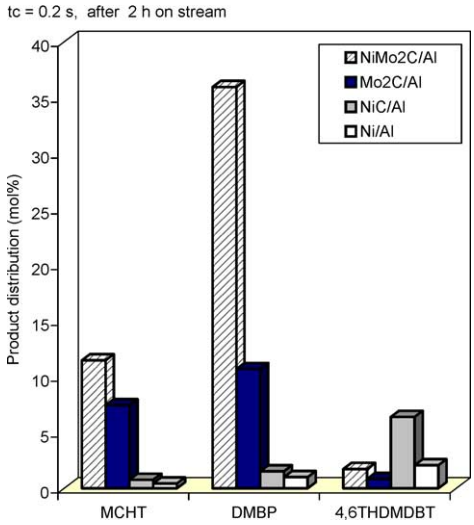

Fig. 5. Product distribution after HDS of 4,6-DMDBT on Ni-doped alumina-supported molybdenum carbide: comparison with Ni-based catalysts and Mo_2C/Al.

pregnation with ammonium heptamolybdate) compared to Mo_2C/Al. The catalyst, $Mo_2CP(0.08)$/Al, derived from the Keggin-type heteropolyacid, $H_3PMo_{12}O_{40}$, is more efficient than the others phosphorus-promoted materials. The P content is low but the rate increase is very large; the HDS rate is 3.81×10^{-6} mol g^{-1} s^{-1} and the selectivity 0.4. In this case, the DDS rate is higher than that of other P-doped alumina-supported molybdenum carbides.

Alumina-supported cobalt- or nickel-doped molybdenum carbides have been studied [23,35]. An enhancement of the catalytic activity for HDS of nonrefractory compounds such as thiophene [35] or dibenzothiophene [23] is observed. The results of DBT hydrodesulfurization [23] over promoted alumina-supported molybdenum carbides show that the reactivity decreases in the order: $NiMo_2C$/Al > $CoMo_2C$/Al > Mo_2C/Al. The major reaction product is biphenyl, as for related sulfided materials. In the present work the HDS of 4,6-DMDBT was studied on $NiMo_2C$/Al. The same kinetic behavior as for Mo_2CP/Al, with two kinetic domains, was observed and the same reaction products (DMBP and MCHT) obtained. The overall HDS rate (4.10×10^{-6} mol g^{-1} s^{-1}) is twice that for Mo_2CP/Al (1.87×10^{-6} mol g^{-1} s^{-1}). The selectivity ratio is lower than with $Mo_2CP(X)$/Al catalysts; the HYD rate is not greatly enhanced but the DDS rate is 3 times higher than with the Mo_2C/Al material.

For comparison, we carried out 4,6-DMDBT HDS with alumina-supported carburized nickel NiC/Al; low activity was observed and the material deactivated in less than 1 h, making kinetic study impossible. Alumina-supported nickel catalyst, Ni/Al, was rapidly sulfided under the reaction conditions and is not active after 2 h on stream. Fig. 5 shows the product distribution following HDS transformation after 2 h on stream and for a contact time of 2 s for all the Ni-based catalysts and for Mo_2C/Al. As observed, the addition of nickel enhances HDS conversion, particularly by the DDS route, which confirms that there is a synergetic effect of nickel in alumina-supported $NiMo_2C$/Al.

All these results contrast with the corresponding sulfided catalysts [25]: more DMBP than MCHT is produced. Therefore, most of the 4,6-DMDBT is desulfurized by direct C–S scission without ring saturation on all the alumina-supported molybdenum carbides whether promoted or not. The effect of phosphorus or nickel promotion may be to increase the acidity of the catalyst. This factor was therefore investigated by XPS and IR.

3.5. Carbide phases and molybdenum oxidation states evidenced by XPS

The distribution of Mo oxidation states for molybdenum oxycarbide was estimated by decomposition of the Mo 3d spectra (Fig. 6). Curve-fitting of Mo 3d peaks was accomplished using linked doublets (Mo $3d_{5/2}$–Mo $3d_{3/2}$) corresponding to three different molybdenum species with binding energies lower than 232.4 eV and higher than 228.0 eV. The XPS results for P-doped materials are summarized in Table 5. A characteristic species with a Mo $3d_{5/2}$ binding energy lower than 229 eV was identified. According to the literature, the binding energy found around 228.2 eV can be attributed to a carbide phase [43] close to molybdenum in a zero-valent state, which is generally found at 227.9 eV in bulk molybdenum carbides [26,44,45]; this Mo species is also close to Mo^{2+} (228.2 ± 0.2 eV) [44,46]. It has been denoted as $Mo^{\delta+}$ and is assumed to be involved in a Mo–C bond. For nondoped alumina-supported molybdenum carbide, 42% of the molybdenum is present in the Mo^0 or $Mo^{\delta+}$ state.

On the contrary, values for P- and Ni-doped catalysts are 13–20 and 32%, respectively. The abundance of this $Mo^{\delta+}$ peak, which is characteristic of a metal-like site, is lower for P- and Ni-containing carbides. However, the hydrogenation and HDS properties are enhanced in the presence of P and Ni. This suggests that while this metal-like species is important for the HDS reactions, an oxycarbide phase which corresponds to a higher oxidation state of molybdenum in the alumina-supported carbides is also required. This molybdenum oxidation state is close to 4+ and to a binding energy of 230.0 eV as observed by Sajkowski et al. [20]. The area of the oxycarbide peaks ranges from 34 to 38% for P/Mo ratios ranging from 0.08 to 0.40, whereas for Mo_2C/Al it is only 23% of the total molybdenum area. The work of Ledoux and co-workers [47–49] has shown the presence of molybdenum atoms mainly as Mo^{5+} and Mo^{4+} in molybdenum oxycarbide; these materials show a high selectivity for alkane isomerization. Similarly, the increase in the oxycarbide phase and, consequently, in the activity can explain the higher activity of our P-containing supported materials in HDS reactions.

For the Ni-containing catalyst, the abundance of $Mo^{\delta+}$ is lower than for Mo_2C/Al but higher than for $Mo_2CP(X)$/Al (with $X = P/Mo$) carbides. Moreover, the area of the molyb-

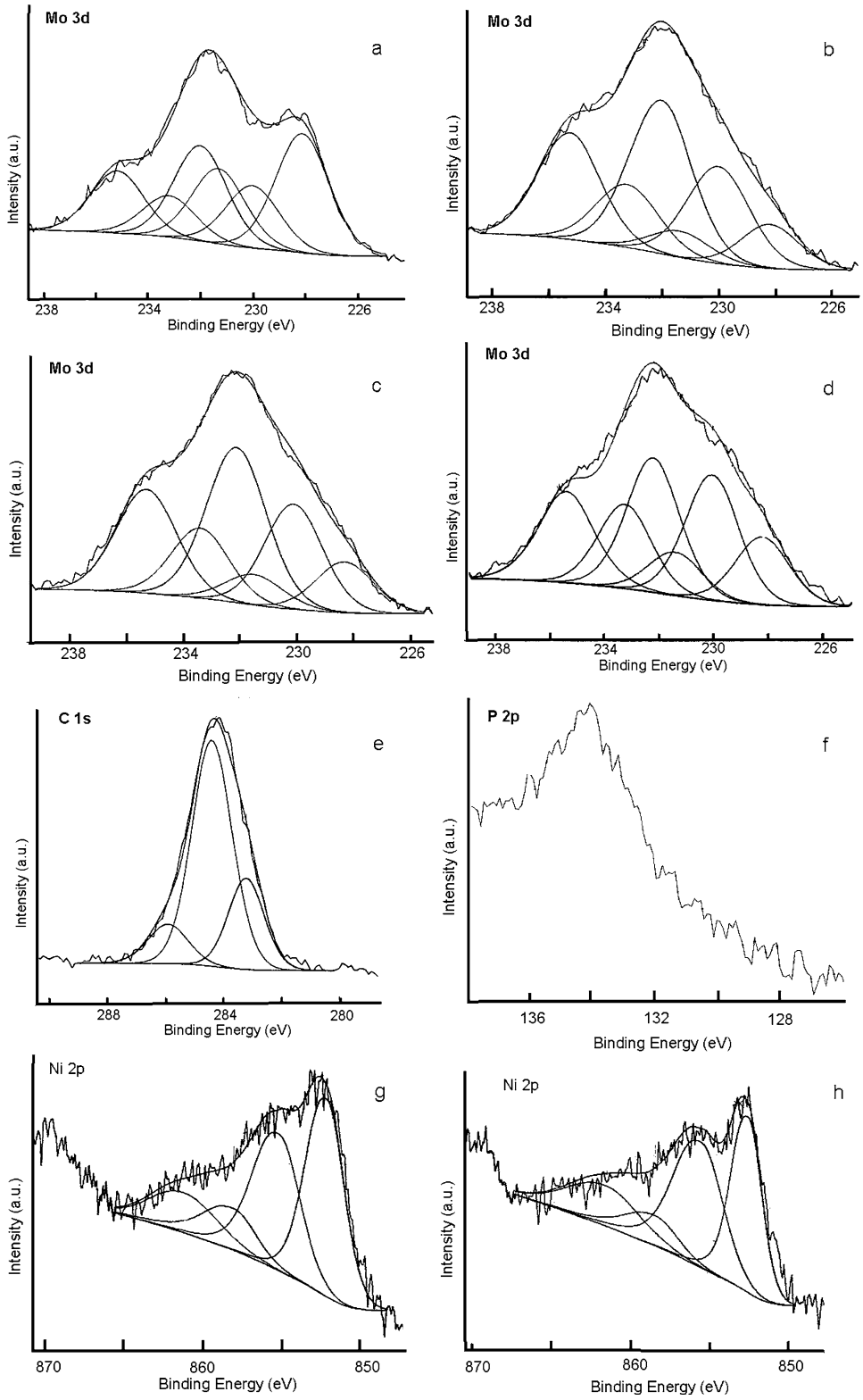

Fig. 6. Superposition of experimental XPS spectra and spectra after decomposition for P-doped alumina-supported molybdenum carbides and Ni-doped molybdenum carbides: Mo 3d (inset) level, (a) P/Mo = 0; (b) P/Mo = 0.08; (c) P/Mo = 0.11; (d) P/Mo = 0.4. C 1s level (e) P/Mo = 0.4. P 2p level (f) P/Mo = 0.4. Ni 2p level (g) NiC/Al; (h) $NiMo_2C$/Al.

Table 5
XPS results for alumina-supported molybdenum carbides with different P/Mo ratios and Ni promoter: Comparison with nondoped material (binding energies (eV) and concentrations (%) of C1s, Mo $3d_{5/2}$, and Ni $2p_{3/2}$ species)

Catalyst	C 1s			Mo $3d_{5/2}$		
	Carbide		Oxicarbide	$Mo^{\delta+}$ carbide	Mo^{4+} oxycarbide	Mo^{6+} oxide
Mo_2C/Al	283.2 (23%)	284.4 (65%)	285.9 (12%)	228.1 (42%)	230.0 (23%)	232.0 (35%)
$Mo_2CP(0.08)$/Al	283.5 (11%)	284.8 (53%)	286.4 (36%)	228.2 (13%)	230.0 (34%)	232.0 (53%)
$Mo_2CP(0.11)$/Al	283.1 (37%)	284.4 (51%)	285.9 (12%)	228.3 (15%)	230.1 (34%)	232.1 (51%)
$Mo_2CP(0.40)$/Al	283.2 (28%)	284.4 (49%)	285.9 (23%)	228.2 (20%)	230.0 (38%)	232.2 (42%)
$NiMo_2C$/Al				228.2 (32%)	230.0 (25%)	232.3 (43%)

	C 1s			Ni $2p_{3/2}$	
	Carbide		Oxicarbide	Oxide	Reduced
$NiMo_2C$/Al	283.3 (17%)	284.5 (28%)	286.0 (55%)	855.5 (56%)	852.5 (44%)
NiC/Al	283.2 (25%)	284.6 (49%)	286.0 (26%)	855.2 (64%)	852.2 (36%)

denum peak involved in the oxycarbide phase (Mo^{4+}) is only 25% of the total molybdenum peak area, which is close to the values found for Mo_2C/Al. The proportions of the various species for Mo_2C/Al and $NiMo_2C$/Al are more similar than for the corresponding P-containing catalysts.

Two peaks at 852.5 and 855.5 eV are observed in the XPS spectrum of Ni $2p_{3/2}$ (Fig. 6 and Table 5) for $NiMo_2C$/Al. The nickel binding energies found are not in agreement with the values reported, neither for nickel sulfide [50,51] nor for nickel oxide [52]. The oxidation state of Ni corresponding to 852.5 eV is assigned to a reduced species higher than 0 and lower than 2+, probably a partial positive charge $\delta+$ ($Ni^{\delta+}$). The Ni $2p_{3/2}$ binding energy at 855.5 eV is attributed to an oxidized Ni^{2+} species. Similar peaks are observed in the XPS spectrum for NiC/Al (Fig. 6g), which suggests that there is supported nickel oxycarbide. The abundance of $Ni^{\delta+}$ in NiC/Al (36%) is lower than that (44%) in $NiMo_2C$/Al. Interaction between nickel and molybdenum could be expected for this latter material; this is consistent with the better tetralin hydrogenation and HDS activities.

For all the alumina-supported molybdenum carbides, the carbon C 1s signal was also decomposed. Three components were found, the lowest binding energy being attributed to carbon from the carbide phase, and this component ranges from 283.1 to 283.5 eV. A second component around 284.5 eV was attributed to adventitious carbon and a third component, at higher binding energy, was attributed to oxidized carbon entities (C–O) [53]. In HDS of 4,6-DMDBT, the overall rate was found to rise as follows: Mo_2C < $Mo_2CP(0.11)$ < $Mo_2CP(0.40)$ < $Mo_2CP(0.08)$. The relative area of the carbon peaks involved in the C–O bond can be ranked in the same sequence in terms of reactivity. We can assume that they are related to the area of the Mo^{4+} (oxycarbide species) peak for alumina-supported molybdenum carbides.

3.6. Acidic properties of molybdenum carbide catalysts

On the IR spectra of all the activated alumina-supported carbides, there is a broad band between 1040 and 980 cm^{-1}, whose shape is difficult to specify due to overlap with the intense vibration bands of the alumina. Treating the activated sample with water shifts the alumina vibration bands to lower frequencies, i.e., outside the observable spectral range. Therefore, the difference between spectra taken after activation and spectra taken after treatment with water reveals two maxima at 1003 and 1021 cm^{-1} in this broad massif (Fig. 7). As reported in the literature [54], impregnation of ammonium heptamolybdate on alumina followed by calcination gives rise to a band at 1005 cm^{-1} characteristic of surface Mo=O species. Therefore, the two bands observed on alumina-supported molybdenum carbides indicate the presence of molybdenum in various environments as an oxidic Mo phase and an oxygen-modified carbide phase. Similar species were also identified by XPS analysis as Mo^{6+} and Mo^{4+} (Table 5). These spectroscopic results confirm that the final materials present some oxygen-containing phases ("oxide" and oxycarbide) rather than pure Mo_2C.

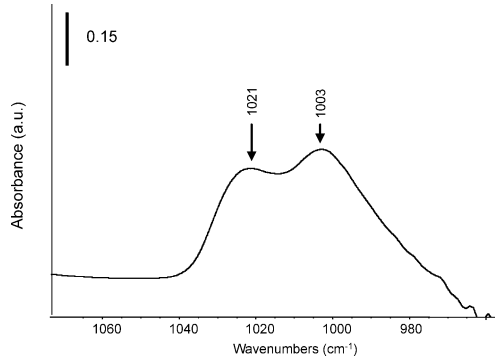

Fig. 7. Difference between spectra of Mo_2C/Al reduced at 773 K taken before and after water treatment at 298 K.

To assess the nature, the number and the strength of the surface sites of the carbide catalysts, the adsorption of a probe molecule was followed by IR spectroscopy. CO and pyridine are the most often used probes [55]. CO presents the advantage of probing both metallic and acidic sites.

On alumina-supported Mo carbides, CO adsorption ($T_{ads} = 295$ K) leads to the appearance of an intense ν(CO) band at 2181 cm^{-1} tailing toward lower frequencies (Fig. 8).

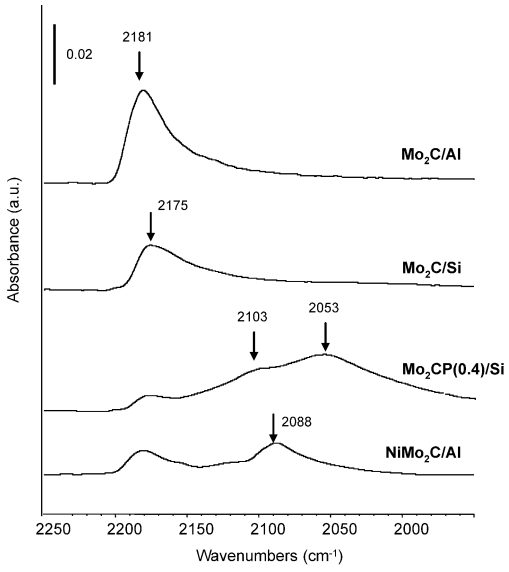

Fig. 8. IR spectra of CO adsorbed (1.333×10^3 Pa equilibrium) on alumina- and silica-supported molybdenum carbides doped with P or Ni.

On the pure alumina support, ν(CO) bands are detected at different values (2230 and 2216 cm^{-1}), which are assigned to weakly chemisorbed CO bonded to coordinately unsaturated Al^{3+} sites (Lewis sites); this is consistent with literature data [56]. Therefore, the band at 2181 cm^{-1} characterizes the supported phase, in agreement with previous results [18] under these conditions. When CO is adsorbed on a silica-supported molybdenum carbide catalyst at RT, it only adsorbs on the supported phase (silica being an inert support) giving rise to a signal very close to that observed on the alumina-supported catalyst (2175 cm^{-1}) (Fig. 8). This confirms that the 2181 cm^{-1} band is a fingerprint of CO adsorbed on Lewis acid sites of the supported phase. This frequency is lower than that detected for CO adsorbed on alumina, indicating that the Lewis acid sites of the carbide catalyst are weaker. Reports on alumina-supported molybdenum oxide show that CO does not adsorb on Mo^{6+}, while on Mo^{5+} and Mo^{4+} the CO signal is detected at about 2200 and 2180 cm^{-1}, respectively [57]. The interaction of CO with metallic Mo gives rise to a band below 2070 cm^{-1} [58]. Previous studies by reflectance absorbance infrared spectroscopy (RAIRS) at 104 K of CO adsorption on clean β-Mo_2C foil report a ν(CO) band at 2057 cm^{-1}, whereas CO adsorption on an oxygen-modified surface (near saturation coverage) results in a broad asymmetric peak with a maximum up to 2076 cm^{-1} [59]. This shift is associated with CO adsorbed on an oxygen-modified molybdenum carbide. Therefore, our CO results indicate that some molybdenum is in an oxide environment, in agreement with the detection of Mo=O bands at 1021–1003 cm^{-1}. These surface Mo species detected by CO are in an oxidation state of +4, as also detected by XPS. In addition to Mo^{4+}, XPS provides also evidence for Mo^{6+} (not detectable by CO [58]) and for $Mo^{\delta+}$ (Table 5). This latter phase is not detected by CO on Mo carbide supported on alumina, no CO vibration appearing in the low wavenumber region. This probably indicates that on the alumina-supported catalyst the surface phase resembles an oxygen-modified carbide. This result is in agreement with previous observations of Aegerter et al. [18]. These authors reported that oxygen adsorbed during the passivation step is not completely eliminated by activation in H_2 at 623 K. An IR band (attributed to CO linearly adsorbed on coordinately unsaturated Mo^{4+} sites) also appears at about 2180 cm^{-1} on passivated alumina-supported molybdenum nitrides reduced at 673 K. These observations suggest that some of the surface Mo sites on the reduced passivated sample are still in a high valence state (Mo^{4+}); i.e., the sample is still a molybdenum oxycarbide. These results are corroborated by very recent experiments of Li and co-workers [60] on a reduced passivated in situ carburized self-supported sample of MoO_3/Al_2O_3.

On the alumina-supported molybdenum carbide doped with phosphorus, a band at 2181 cm^{-1} is also observed. Similarly and in agreement with XPS data, an oxygen-modified carbide phase is also present in these catalyts.

On the Ni-doped catalyst, the band at 2181 cm^{-1} is still detected, but it is weaker than for the pure Mo catalyst, and two bands at about 2120 and 2088 cm^{-1} are also observed (Fig. 8). Therefore, both acid and metallic sites occur on alumina-supported NiMo carbide. On NiC/Al, a weak ν(CO) band is observed at 2187 cm^{-1} while the main band appears at 2096 cm^{-1}. Moreover, the slight difference ($\Delta\nu = 8$ cm^{-1}) between the low-frequency band on NiC/Al and on $NiMo_2C$/Al indicates that the electronic properties of NiC are modified by the presence of Mo in the latter (interaction between Mo and Ni). Similar trends are observed for CO adsorption on alumina-supported sulfided NiMo catalysts. A signal due to CO interacting with sulfided Ni/Al is observed at 2085 cm^{-1} whereas on NiMoS/Al new bands appear at 2078 cm^{-1} (leading to an equivalent shift $\Delta\nu = 7$ cm^{-1}) and 2120 cm^{-1}, indicating an interaction between Ni and Mo [61].

To further characterize the acidic sites of supported carbide catalysts, pyridine was also used as probe molecule. Pyridine can coordinate on Lewis acid sites while it is protonated on sufficiently acidic protic sites.

On the alumina-supported molybdenum carbide catalysts, the interaction of pyridine followed by evacuation at 473 K gives several bands at about 1622, 1608 (sh), 1577, 1494, and 1452 cm^{-1} (Fig. 9). These bands are characteristic of Lewis acid sites [52]. No peak corresponding to Brønsted acid sites (1540 cm^{-1}) is observed. In the 1625–1600 cm^{-1} region, two bands (at 1622 and 1608 cm^{-1}) indicate Lewis acid sites of strong and medium acid strength, respectively. Comparison with pure alumina shows that the peak at 1622 cm^{-1} can be attributed to pyridine coordinated on unsaturated surface Al^{3+} sites of the support [62] while that at 1608 cm^{-1} could be attributed to the supported phase. When pyridine was adsorbed at 473 K on silica-supported carbide catalyst, only the peak at 1608 cm^{-1} was detected. This confirms that there are weak Lewis acid sites located

on the oxygen-modified carbide, as detected by CO. Comparison with previous results [63] shows that the Lewis acid sites are stronger on the oxygen-modified molybdenum carbide ($\nu \sim 1608$ cm^{-1}) than on the molybdenum sulfided ($\nu \sim 1600$ cm^{-1}).

On P-doped carbide catalysts supported on alumina, the intensity of the band for acid sites (1608 cm^{-1}) increases with the amount of P (Fig. 9). No Brønsted acidic sites are detected. Thus, the increase in the number of Lewis sites in the presence of phosphorus indicates an enhancement of the proportion of Mo in an oxide environment or coordinately unsaturated (anionic vacancy). These results are in agreement with XPS analysis, which shows an increase in the proportion of Mo^{4+} and Mo^{6+} on P-doped catalysts (Table 5). For the Ni-containing catalyst, the pyridine spectrum also presents a shoulder at around 1608 cm^{-1} of intensity similar to that in the absence of Ni (Fig. 9). This indicates that the Ni-containing carbide is less acidic than the P-doped carbides.

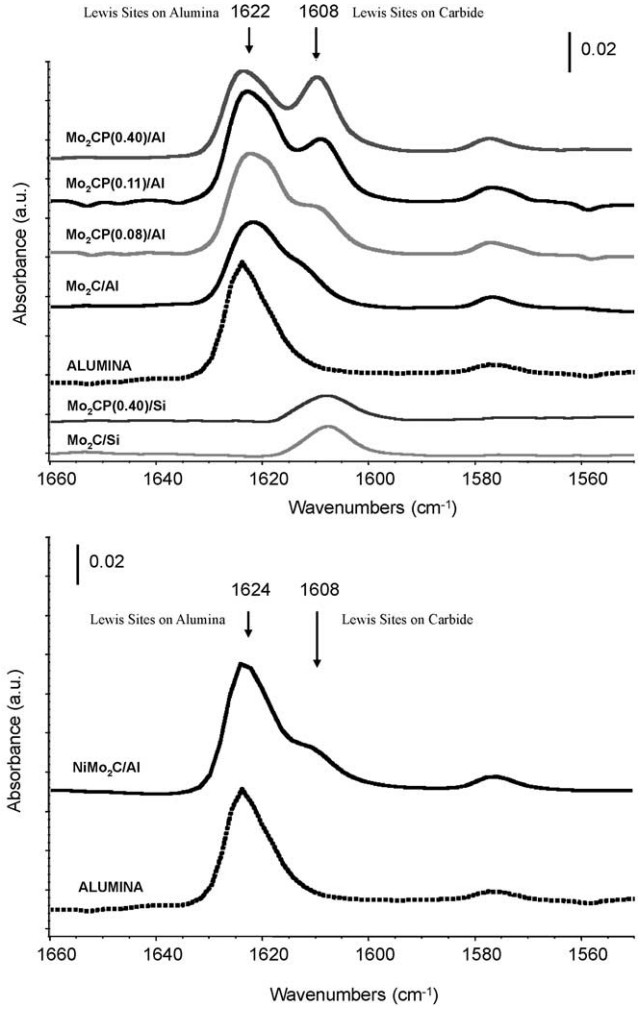

Fig. 9. IR spectra of species resulting from pyridine evacuation at 473 K on various P-doped alumina-supported molybdenum carbides: comparison with silica-supported and Ni-doped alumina-supported molybdenum carbides.

4. Discussion

The pyridine FTIR results, for nonpromoted and P-doped carbide catalysts supported on alumina, show that the intensity of the band at 1608 cm^{-1}, characteristic of coordination sites, increases with the amount of P. The addition of P increases the number of Lewis sites in the carbide phase and enhances the Mo^{4+} abundance, as observed by XPS analysis (Table 5). The peak area at 1608 cm^{-1} is linearly correlated with the abundance of the Mo^{4+} oxidation state given by XPS analysis (Fig. 10a). When the DDS rates are plotted against the Mo^{4+} abundance (Fig. 10b), only the $Mo_2CP(0.08)$ datum is not correlated. These results indicate that Mo^{4+} are active centers for 4,6-DMDBT hydrodesulfurization on alumina-supported molybdenum carbides.

On the contrary, for Ni-doped catalysts, no correlations are observed. The Mo^{4+} abundance, which is related to the

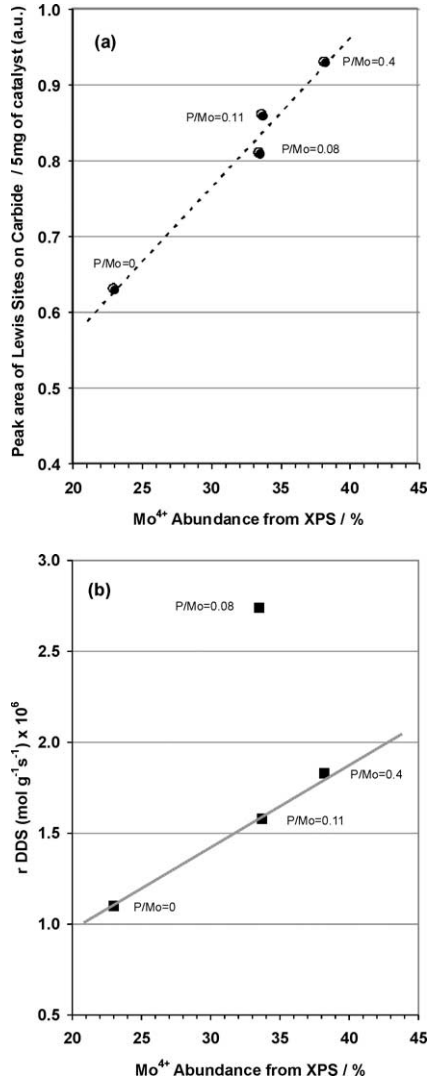

Fig. 10. (a) Relationship between peak area at 1608 cm^{-1} (pyridine IR spectra) and Mo^{4+} abundance from XPS spectra of alumina-supported molybdenum carbides; (b) relationship between DDS rate and Mo^{4+} abundance from XPS spectra of alumina-supported molybdenum carbides.

DDS pathway for the P-promoted carbides, is only 25% of the total molybdenum abundance. The IR pyridine spectrum also presents a shoulder at around 1608 cm^{-1} but its intensity is quite similar to that measured on the nonpromoted catalyst (Fig. 9), in agreement with the Mo^{4+} level detected by XPS. The $Mo^{\delta+}$ abundance is lower than for a nonpromoted catalyst but higher than for P-containing materials. Nevertheless, the NiMoC/Al catalyst gives the highest overall and DDS rates for 4,6-DMDBT HDS; therefore, the sites involved for the P-promoted alumina-supported molybdenum carbides do not explain the high activity of these materials. However, CO FTIR experiments reveal synergetic effects resulting from complex chemical combinations of Ni and molybdenum carbides on alumina as for NiMoS/Al; "Ni-Mo-C" entities can also be envisaged in our case, but more studies are needed.

Under conventional HDS conditions (613 K, 4 MPa total pressure) and for alumina-supported sulfided molybdenum catalysts, the DDS pathway contributes only 8% to the HDS of 4,6-DMDBT; Ni promotion enhances the DDS pathway (20%), this latter remaining minor [10]. Kwak et al. [15] have reported that in 4,6-DMDBT HDS, phosphorus addition to CoMoS/Al increases the conversion and promotes DDS more than HYD, though HYD is still the more important. The number of Brønsted acid sites increases with the amount of phosphorus, while the numbers of Lewis acid sites remains almost unchanged. These differences are caused by the acid treatment of the support prior to impregnation. Increase in the Brønsted acidity favors the migration of the methyl group in 4,6-DMDBT, so that the aromatic ring and the C–S–C bridge becomes more accessible to the active sites.

No such mechanism can be expected in our case; as reported in this work, Lewis acid sites are the most active species for HDS of 4,6-DMDBT. Recently the decomposition of isopropanol and the temperature-programmed desorption of CO_2 and NH_3 have been employed to evaluate the acid–base properties of molybdenum carbides [64]. To explain the appearance of acid and basic sites, the authors proposed the development of Lewis acid and base character over the Mo and C atoms, respectively. The similarity to the proposals of Bataille et al. [10] for MoS_2/Al is remarkable: negative charge on sulfur for sulfide and on carbon for carbide, incompletely coordinated molybdenum atoms (Lewis acid) in both materials. Therefore, we propose a mechanism based on that of Bataille et al. [10] for C–S bond cleavage of 4,6-DMDBT. The first step is the hydrogenation of the double bond in the vicinity of the sulfur atom of the organic molecule; the second step (for the DDS pathway) is the opening of the C–S bond by an elimination process, which involves the attack of a hydrogen atom at the β position relative to the sulfur atom by a carbon of the supported molybdenum carbide acting as a basic site. The main effect of the phosphorus is presumably to increase the basicity of the carbide carbons atoms.

The data obtained in this study provide the basis for the design of an optimal catalyst with high efficiency in deep desulfurization.

5. Conclusions

The influence of phosphorus and nickel on the properties of alumina-supported molybdenum carbides was determined by XPS and IR, and also evidenced in 4,6-DMDBT hydrodesulfurization

The hydrodesulfurization of 4,6-DMDBT hydrodesulfurization occurs through two different coupled routes: direct DDS and HYD. The overall conversion of 4,6-DMDBT as well as the DDS and HYD routes are zero order in reactant for contact times lower than 0.4 s and for conversions lower than 45%.

No difference in the kinetics was found between Ni- or P-promoted and nonpromoted catalysts. A mechanistic scheme involving coupled catalytic cycles and a unique adsorbed species common to both cycles was proposed.

The selectivity ratio (r_{HYD}/r_{DDS}) indicates that the direct desulfurization route is favored over alumina-supported molybdenum carbides, in contrast with alumina-supported sulfided molybdenum or nickel-molybdenum.

The XPS analysis shows that the abundance of Mo^{4+} increases with P addition; this enhancement is correlated with the peak area of the 1608 cm^{-1} band (attributed to Lewis acid sites) observed in pyridine IR spectra. Furthermore, the DDS rate is related to the Mo^{4+} abundance. Therefore, Lewis acid sites are the key to the increased activity in the DDS pathway. From these results, it appears possible to tune the Mo^{4+} fraction to maximize HDS activity.

Pyridine IR spectra can be correlated with HDS activity, and lead to the following ranking for the overall HDS rate: $Mo_2C < Mo_2CP(0.11) < Mo_2CP(0.40) < Mo_2CP(0.08)$.

For the nickel-promoted catalysts, IR spectroscopy of adsorbed CO indicates an interaction between nickel and molybdenum, as observed in NiMoS/Al, which explains its high activity.

Acknowledgments

This work was carried out in the framework of the program Post-traitement de coupes gazoles hydrotraitées supported by Elf, IFP, Total, Procatalyse, and CNRS-ECODEV. The authors are particularly grateful to G. Pérot and J.-L. Lemberton who contributed to this work. Thanks are due to Mrs. P. Beaunier for the EDS measurements and to Dr. J.S. Lomas for fruitful discussions and for correcting the manuscript.

References

[1] T. Kabe, A. Ishihara, H. Tajima, Ind. Eng. Chem. Res. 31 (1992) 218.
[2] A. Ishihara, H. Tajima, T. Kabe, Chem. Lett. (1992) 669.

[3] X. Ma, K. Sakanishi, T. Isoda, I. Mochida, Ind. Eng. Chem. Res. 34 (1995) 748.
[4] D.H. Kilanowski, H. Teeuwen, V.H.J. De Beer, B.C. Gates, G.C.A. Schuit, H. Kwart, J. Catal. 55 (1978) 129.
[5] D.D. Whitehurst, T. Isoda, I. Mochida, Adv. Catal. 42 (1998) 345.
[6] M.V. Landau, Catal. Today 36 (1997) 393.
[7] G.H. Singhal, R.L. Espino, J.-E. Sobel, G.A. Huff, J. Catal. 67 (1981) 457.
[8] M. Houalla, N.K. Nag, A.V. Sapre, D.H. Broderick, B.C. Gates, AIChE J. 24 (1978) 1015.
[9] M. Meille, E. Schulz, M. Lemaire, M. Vrinat, J. Catal. 170 (1997) 457.
[10] F. Bataille, J.-L. Lemberton, P. Michaud, G. Pérot, M. Vrinat, M. Lemaire, E. Schulz, M. Breysse, S. Kasztelan, J. Catal. 191 (2000) 409.
[11] M. Macaud, A. Milenkovic, E. Schulz, M. Lemaire, M. Vrinat, J. Catal. 193 (2000) 255.
[12] H. Topsøe, B.S. Clausen, F.E. Massoth, Hydrotreating Catalysis, Springer, Berlin, 1996.
[13] R. Prins, Adv. Catal. 46 (2002) 399.
[14] R. Iwamoto, J. Grimblot, Adv. Catal. 44 (2000) 417.
[15] C. Kwak, M.Y. Kim, K. Choi, S.H. Moon, Appl. Catal. A 185 (1999) 19.
[16] A. Griboval, P. Blanchard, E. Payen, M. Fournier, J.-L. Dubois, in: G.F. Froment, B. Delmon, P. Grange (Eds.), Hydrotreatment and Hydrocracking of Oil Fractions, Elsevier, Amsterdam, 1997, p. 181.
[17] A. Griboval, P. Blanchard, E. Payen, M. Fournier, J.-L. Dubois, Catal. Today 45 (1998) 277.
[18] P.A. Aegerter, W.W.C. Quigley, G.J. Simpson, D.D. Ziegler, J.W. Logan, K.R. McCrea, S. Glazier, M.E. Bussell, J. Catal. 164 (1996) 109.
[19] K.R. McCrea, J.W. Logan, J.L. Tarbuck, M.E. Heiser, M.E. Bussell, J. Catal. 171 (1996) 255.
[20] D.J. Sajkowski, S.T. Oyama, Appl. Catal. A 134 (1996) 339.
[21] B. Dhandapani, T.St. Clair, S.T. Oyama, Appl. Catal. A 168 (1998) 219.
[22] S. Li, J.S. Lee, J. Catal. 178 (1998) 119.
[23] H.K. Park, D.S. Kim, K.L. Kim, Korean J. Chem. Eng. 15 (1998) 625.
[24] P. Da Costa, J.-L. Lemberton, C. Potvin, J.-M. Manoli, G. Pérot, M. Breysse, G. Djéga-Mariadassou, Catal. Today 65 (2001) 195.
[25] P. Da Costa, C. Potvin, J.-M. Manoli, M. Breysse, G. Djéga-Mariadassou, Catal. Lett. 86 (2003) 133.
[26] P. Perez-Romo, C. Potvin, J.-M. Manoli, M.M. Chehimi, G. Djéga-Mariadassou, J. Catal. 208 (2002) 187.
[27] R. Contant, in: P. Ginsberg (Ed.), Inorganic Syntheses, Wiley, New York, 1990, p. 104.
[28] R. Strandberg, Acta Chem. Scand. 27 (1973) 1004.
[29] P. Da Costa, C. Potvin, J.-M. Manoli, M. Breysse, G. Djéga-Mariadassou, Catal. Lett. 72 (2001) 91.
[30] J.-L. Lemberton, M. Cattenot, V. Kougionas, M. Mahouer, J.-L. Portefaix, M. Breysse, G. Perot, in: G.F. Froment, B. Delmon, P. Grange (Eds.), Hydrotreatment and Hydrocracking of Oil Fractions, Elsevier, Amsterdam, 1997, p. 529.
[31] R.L. Burwell, Langmuir 2 (1986) 2.
[32] J.E. Germain, R. Maurel, C. R. Acad. Sci. 247 (1958) 1854.
[33] M.P. Seah, in: D. Briggs, M.P. Seah (Eds.), Practical Surface Analysis by Auger and X-Ray Photoelectron Spectroscopy, Vol. 1, Wiley, New York, 1990, pp. 225–226, Chap. 5.
[34] T.-C. Xiao, A.P.E. York, H. Al-Megren, C.V. Williams, H.T. Wang, M.L.H. Green, J. Catal. 202 (2001) 10.
[35] M.E. Bussell, P. Mills, B.P. Woodruff, R. Main, D.C. Phillips, Prep. Am. Chem. Soc., Div. Petrol. Chem. 44 (1999) 206.
[36] J.S. Lee, K.H. Lee, J.Y. Lee, J. Phys. Chem. 96 (1992) 362.
[37] B. Dhandapani, S. Ramanathan, C.C. Yu, B. Frühberger, J.G. Chen, S.T. Oyama, J. Catal. 176 (1998) 61.
[38] M. Vrinat, Appl. Catal. 6 (1983) 137.
[39] V. Meille, E. Schulz, M. Lemaire, M. Vrinat, Appl. Catal. A 187 (1999) 179.
[40] M. Houalla, D.H. Broderick, A.V. Sapre, N.K. Nag, V.H.J. de Beer, B.C. Gates, J. Kwart, J. Catal. 61 (1980) 523.
[41] P. Da Costa, C. Potvin, J.-M. Manoli, J.-L. Lemberton, G. Pérot, G. Djéga-Mariadassou, J. Mol. Catal. A 184 (2002) 323.
[42] M. Boudart, G. Djéga-Mariadassou, Kinetics of Heterogeneous Catalytic Reactions, Princeton Univ. Press, Princeton, 1984.
[43] M.J. Ledoux, C. Pham-Huu, J. Guille, H. Dunlop, J. Catal. 134 (1992) 383.
[44] J.G. Choi, L.T. Thompson, Appl. Surf. Sci. 93 (1996) 143.
[45] J.G. Choi, J.R. Brenner, C.W. Colling, J.L. Demczyk, J.L. Dunning, L.T. Thompson, Catal. Today 15 (1992) 201.
[46] R.B. Quincy, M. Houalla, A. Proctor, D.M. Hercules, J. Phys. Chem. 94 (1990) 1520.
[47] P. Delporte, F. Meunier, C. Pham-Huu, P. Vennegues, M.J. Ledoux, J. Guille, Catal. Today 23 (1995) 2511.
[48] P. Delporte, C. Pham-Huu, M.J. Ledoux, J. Chim. Phys. 93 (1996) 507.
[49] C. Bouchy, C. Pham-Huu, B. Heinrich, C. Chaumont, M.J. Ledoux, J. Catal. 190 (2000) 92.
[50] M. Sun, T. Bürgi, R. Cattaneo, D. Van Legeveld, R. Prins, J. Catal. 201 (2001) 258.
[51] C.D. Wagner, W.M. Riggs, L.E. Davis, J.F. Moulder, G.E. Muilenberg, Handbook of X-Ray Photoelectron Spectroscopy, Perkin–Elmer, Palo Alto, CA, 1979.
[52] K.T. Ng, D.M. Hercules, J. Phys. Chem. 80 (1976) 2094.
[53] Z. Paal, X.L. Xu, J. Paal-Lukacs, W. Vogel, M. Muhler, R. Scholg, J. Catal. 152 (1995) 252.
[54] M. Cornac, A. Janin, J.-C. Lavalley, Infrared Phys. 24 (1984) 143.
[55] E. Payen, J. Grimblot, J.-C. Lavalley, M. Daturi, F. Maugé, in: J.M. Chalmers, P.R. Griffith (Eds.), Handbook of Vibrational Spectroscopy, Vol. 4, Wiley, New York, 2002, p. 3005.
[56] C. Morterra, G. Magnacca, Catal. Today 27 (1996) 497.
[57] C. Louis, L. Marchese, S. Coluccia, A. Zecchina, J. Chem. Soc., Faraday Trans. 1 85 (1998) 1655.
[58] N. Sheppard, T.T. Nguyen, Adv. IR Raman Spectrosc. 5 (1978) 67.
[59] J. Wang, M. Castonguay, J. Deng, P.H. MacBreen, Surf. Sci. 374 (1997) 197.
[60] W. Wu, Z. Wu, C. Liang, X. Chen, P. Ying, C. Li, J. Phys. Chem. B 107 (2003) 7088.
[61] M. Angulo, F. Maugé, J.-C. Duchet, J.-C. Lavalley, Bull. Soc. Chim. Belg. 96 (1987) 925.
[62] C. Lahousse, A. Aboulayt, F. Maugé, J. Bachelier, J.-C. Lavalley, J. Mol. Catal. 84 (1993) 283.
[63] G. Berhault, M. Lacroix, M. Breysse, F. Maugé, J.-C. Lavalley, H. Nie, L. Qu, J. Catal. 178 (1998) 555.
[64] S.K. Bey, A.C. Bennett, L.T. Thompson, Appl. Catal. A 241 (2003) 1.